ARCHIVES OF MECHANICS
Arch. Mech. **77** (6), 647–678, 2025, https://doi.org/10.24423/aom.4789

# Thermophoresis of a cylindrical particle embedded in a porous medium saturated by a micropolar fluid

S. NISHAD, K. P. MADASU*)

*Department of Mathematics, National Institute of Technology Raipur, 492010, Chhattisgarh, India,*
*e-mails: snishad.phd2022.maths@nitrr.ac.in, madaspra.maths@nitrr.ac.in, kpm973@gmail.com (corresponding author)*

The present study examines the thermophoresis of a cylindrical particle in a direction perpendicular to its axis in the Brinkman medium. To describe the behaviour of micropolar fluid driven by a thermal gradient within such a porous medium, the modified Brinkman's equation is applied while considering low Reynolds and Péclet numbers. The governing equations for both the particle and the medium are solved using the separation of variables technique. The boundary conditions applied at the particle surface are thermal jump and heat flux continuity, with viscous slip, thermal creep, thermal stress slip and microrotation slip. The main objective of the research is to derive the expressions for thermophoretic velocity and thermophoretic force of a cylindrical particle. Graphical representations illustrate the thermophoretic velocity and force of the particle for various physical parameters, including the permeability, micropolarity parameter, thermal stress slip parameter, viscous slip parameter, Knudsen number, and thermal conductivity parameters. The results show that an increase in the micropolarity parameter decreases both the thermophoreti velocity and the force. Additionally, thermophoretic velocity increases with higher permeability, while the thermophoretic force decreases with increasing permeability and the thermal conductivity ratio. The findings of this research align with previously published studies and hold potential applications in industrial processes, including filtration, heat exchangers, air cleaning, and manufacturing thermal precipitators.

**Key words:** thermophoresis, cylindrical particle, micropolar fluid, porous medium.



## Notation

$a$ radius of circular cylinder [m],
$k_p$ thermal conductivity of the particle [$\mathrm{W \cdot m^{-1} \cdot K^{-1}}$],
$k_A$ thermal conductivity of the medium [$\mathrm{W \cdot m^{-1} \cdot K^{-1}}$],
$T_p$ the temperature distribution for the cylindrical particle [K],
$T$ the temperature distribution for the porous medium [K],
$E_\infty$ the prescribed thermal gradient in the absence of the particle [$\mathrm{K \cdot m^{-1}}$],
$C_t$ the thermal jump coefficient of the particle surface,
$C_m$ the frictional slip coefficient at the particle surface,
$C_s$ the thermal creep coefficient at the particle surface,

$C_h$ the thermal stress slip coefficient at the particle surface,
$C_n$ the microrotation slip coefficient at the particle surface,
$k_1$ the permeability [$\mathrm{m}^2$],
$u_\rho$, $u_\theta$ velocity components in cylindrical coordinates [$\mathrm{m} \cdot \mathrm{s}^{-1}$],
$\vec{u}$ fluid velocity [$\mathrm{m} \cdot \mathrm{s}^{-1}$],
$U$ uniform velocity of the particle [$\mathrm{m} \cdot \mathrm{s}^{-1}$],
$T_0$ absolute temperature at the position of particle center in the absence of the particle [K],
$T_\infty$ prescribed temperature distribution in the absence of the particle [K],
$F$ drag force exerted on the cylindrical particle [N],
$F_T$ thermophoretic force [N],
$l$ mean free path of the gas molecules [m],
$p$ pressure [$\mathrm{N} \cdot \mathrm{m}^{-2}$],
$\vec{e}_\rho$, $\vec{e}_\theta$, $\vec{e}_z$ unit vectors in $\rho$, $\theta$ and $z$ directions,
$U_T$ thermophoretic velocity [$\mathrm{m} \cdot \mathrm{s}^{-1}$],
$K_n(*)$ the modified Bessel's function of order $n$.

## Greek symbols

$\mu$ viscosity of classical fluid [$\mathrm{kg} \cdot \mathrm{m}^{-1} \cdot \mathrm{s}^{-1}$],
$\kappa_p$ rotational coefficient [$\mathrm{kg} \cdot \mathrm{m}^{-1} \cdot \mathrm{s}^{-1}$],
$\alpha_0$, $\beta_0$, $\gamma_0$ gyroviscosity coefficients of micropolar fluid [$\mathrm{kg} \cdot \mathrm{m} \cdot \mathrm{s}^{-1}$],
$\vec{\nu}$ microrotation vector [$\mathrm{rad} \cdot \mathrm{s}^{-1}$],
$\vec{\omega}$ vorticity vector [$\mathrm{rad} \cdot \mathrm{s}^{-1}$],
$\rho_A$ density of the fluid [$\mathrm{kg} \cdot \mathrm{m}^{-3}$],
$\varphi$ porosity of the porous medium,
$\rho$ radial cylindrical coordinate [m],
$\theta$ angular cylindrical coordinate,
$\nabla^2$ Laplacian operator,
$\Pi_{\rho\rho}$, $\Pi_{\rho\theta}$ normal and shear stresses in fluid phase [$\mathrm{N} \cdot \mathrm{m}^{-2}$],
$\psi$ Stokes stream function of the fluid [$\mathrm{m}^3 \cdot \mathrm{s}^{-1}$].

## 1. Introduction

THERMOPHORESIS IS THE MOTION OF PARTICLES in a gaseous medium that arises due to a temperature gradient. When a temperature difference forms in a medium with suspended particles, these particles tend to migrate from hotter regions to colder ones. This mechanism is known as thermophoresis. The study of thermophoresis has received significant interest from researchers because of its wide range of applications, which includes air purification, protection of nuclear reactors, manufacturing of electronic devices, and the removal of soot particles from combustion emissions [1, 2]. In thermophoresis, molecules in the hotter region of the fluid medium possess more energy and have a stronger influence on particles than those in the colder region, causing them to migrate in the opposite direction of the thermal gradient [3]. The Knudsen number is a significant parameter for the study of thermophoresis phenomena, and it is denoted as $K_n = l/a$ ($l$ and $a$ represent the particle's mean free path and characteristic

length, respectively). The totally immersed solid particle is surrounded by a narrow fluid layer called the Knudsen layer, which flows along the direction of the ambient temperature gradient.

In recent years, many authors have elaborated on the thermophoresis theory in Newtonian fluids by adopting the geometries such as spheres, spheroids, cylinders, parallel plates, microtubes, etc. In 1962, BROCK [4] analyzed the thermophoresis of an aerosol sphere using a perturbation technique. CHANG and KEH [5] investigated the thermophoretic migration of a solid sphere under the consideration of thermal stress slip condition. Using the perturbation technique, CHANG and KEH [6], and TSENG and KEH [7] investigated the thermophoresis of a spherical and a cylindrical particles by assuming a non-zero Péclet number. KEH and CHANG [8] examined the thermophoresis phenomenon of a spheroid particle in the direction of axis of revolution. KEH and TU [9] obtained the analytical formulas for the thermophoretic movement of a solid cylinder along the normal direction to its axis. CHANG and KEH [10] analyzed the thermal stress slip effect on the motion of a solid cylinder under thermal gradient. They found the thermal stress slip can enhance or reduce the thermophoretic velocity, depending on the physical and interfacial characteristics of both the medium and particle. WANG and KEH [11] discussed the effects of boundary on thermophoresis of an aerosol cylinder along the direction of perpendicular and parallel to their axis. LU and LEE [12] analyzed the migration of a solid sphere within a nonconcentric pore under non-unifrom thermal environment. KEH and CHEN [13] investigated the parallel thermophoretic movement of an aerosol spherical particle between two plane walls. Also, KEH and CHANG [14] considered the motion of an aerosol sphere in a normal direction between two plane walls under a temperature gradient.

A porous medium refers to a structure composed of interconnected voids and solid spaces. The movement of fluids through porous materials is essential for numerous scientific, engineering, and technological purposes. This kind of fluid flow is particularly important in areas such as geothermal energy, fiber and granular insulation, and particle sedimentation [15–17]. YADAV and DEO [18] considered the problem of incompressible, steady flow of Newtonian fluid through a porous spheroid immersed in another porous medium. RAGAB *et al.* [19] conducted a theoretical study using the boundary collocation scheme to discuss the axisymmetric migration of a colloidal sphere in the Brinkman medium. Their research specifically focused on the movement of the sphere near a bounding wall under the influence of a temperature gradient. FALTAS and RAGAB [20, 21] examined the problems of thermophoresis of particles (spherical and cylindrical) in the Brinkman medium. FALTAS *et al.* [22] analyzed the thermophoresis of a spherical particle between two permeable channels. PRASANNAKUMARA *et al.* [23] conducted a discussion on two-dimensional laminar flow through the Brinkman

medium with the thermophoresis effect. Faltas *et al.* [24] discussed the movement of a solid sphere embedded within the Brinkman medium under the condition of a non-vanishing Péclet number. Huang and Hsu [25] analyzed the mechanism of thermal transport of aerosol particles in a viscous fluid having variable viscosity. Nishad and Madasu [26] discussed the thermophoretic movement of a solid cylinder in a cylindrical cavity using the Brinkman model.

The concept of micropolar fluids was proposed by Eringen [27], which accounts for the effects of microstructure and the rotational dynamics of fluid particles. There are many applications in the fields of science, engineering, and industry for this theory. The Navier–Stokes equations of classical fluid dynamics do not account for the behaviour of fluids with microstructure. Eringen [27] developed the theory of micropolar fluid to model such types of fluids. El-Sapa *et al.* [28] performed an analytical study on unsteady, time-periodic flow of a micropolar fluid through a porous media in a cylindrical microannulus. Saad and Faltas [29, 30] have explored several interesting problems involving thermophoretic transport of spherical particles in micropolar fluid. Roja *et al.* [31] discussed the thermophoretic migration of suspended particles in micropolar fluids while considering the influence of the magnetohydrodynamics. Liu *et al.* [32] examined the thermophoretic migration of nanoparticles in the transition regime using molecular dynamics simulations. Nishad and Madasu [33] analyzed the effects of boundary and micropolarity on the movement of a spherical particle in micropolar fluid within a spherical cavity under thermal gradient. Sarma *et al.* [34] discussed the impacts of thermophoresis, Brownian motion, and non-uniform heat sources on the Maxwell nanofluid flow through a vertical cylinder.

Recent studies on flow of non-Newtonian fluids through porous media have become a vital research area, providing insights capable of tackling a variety of complex fluid dynamics challenges. This field of study has promising applications in several industries, including oil and petroleum, where understanding fluid flow can enhance extraction efficiency. Additionally, it plays a vital role in chemical filtration processes, where the flow of fluids through porous filters is essential for effective separation. This concept is also important in biomedical applications, particularly for understanding blood flow through porous vascular structures, which are crucial for developing improved treatments for various circulatory ailments. Singh and Yadav [35] conducted an analysis on the modeling of blood trihybrid nanofluid flow through porous branched-type arteries that exhibit stenoses and aneurysms. They employed a finite difference approach for the analysis. Srivastava and Yadav [36] examined the mixed convection of couple stress fluid flow through arrays of vertical cylinders, which are enclosed by a homogeneous permeable wall. Abd-Alla *et al.* [37] investigated the peristaltic flow problem of a micropolar fluid through a porous medium.

They explored the impact of coupling number, Hartmann number, micropolar parameter, permeability on velocity, temperature and microrotation using ND solve Mathematica. KHAN and SULAIMAN [38] examined the incompressible mixed convection flow of a micropolar fluid under an electric field and thermal non-equilibrium within a vertical circular porous medium (pipe) utilizing the non-Darcy–Brinkman–Forchheimer model. KAUSAR *et al.* [39] conducted a computational analysis of micropolar fluid flow in porous media over a stretchable sheet, accounting for chemical reaction, thermal radiation, and viscous dissipation. AHAMEDSHERIFF *et al.* [40] studied Soret and Dufour effects on magneto micropolar fluid flow past a stretching sheet in a permeable medium. KUMAR and YADAV [41] discussed the immiscible flow of couple stress and micropolar fluids through a permeable channel, considering the effects of thermal radiation and magnetic field. This type of study has applications in the design of electronic devices and optimizing the efficiency of thermal power systems. KUMAR *et al.* [42] studied the flow of micropolar fluid over a stretching sheet in the non-Darcy permeable medium, taking into account the Soret–Dufour effects, Hall current, magnetic effect, and chemical reactions. In view of the thermophoresis theory, NISHAD and MADASU [43] investigated the thermophoresis of a spherical particle in a porous medium saturated with a micropolar fluid. Recently, NISHAD and MADASU [44] have discussed the effects of micropolarity parameter, permeability, and separation parameter on the thermophoretic movement of a solid sphere in the Brinkman non-Newtonian fluid within a cavity.

The studies previously discussed in the literature focus on the flow of non-Newtonian fluids through porous media, examining various effects such as thermophoresis, magnetic fields, and thermal radiation. Some research is conducted under specified surface temperature boundary conditions, while others employ non-Newtonian heating thermal boundary conditions. In this paper, the authors concentrate on the thermophoretic transport of a cylindrical particle embedded in the Brinkman medium that consists of a micropolar fluid. The key contribution of this research is to derive the expressions for the thermophoretic velocity and force of the cylindrical particle. In this study, we examine the impacts of various factors, including thermal properties, micropolarity parameter, permeability, viscous slip, thermal stress slip, and thermal jump parameter on the thermophoretic velocity and force of a solid cylindrical particle immersed in a micropolar fluid. This work extends the study of NISHAD and MADASU [43] to the case of a cylindrical particle. Aerosol particles, which can take various shapes such as spheres, cylinders, and spheroids, contribute significantly to environmental pollution. In our research, we focus on cylindrical aerosol particle to analyze their behaviour in a micropolar fluid of porous medium. The findings show that the migration of the particle is affected by the micropolar and permeability characteristics of the medium. Understanding this topic can help

industrial fields effectively remove small dust particles from precipitators and filters that undergo temperature gradients. However, this study does not consider several situations, such as the unsteady flow of micropolar fluid, high Reynolds number, or non-zero Péclet number. Additionally, this work does not consider inhomogeneous porous media or the impacts of magnetic field, concentration, Brownian motion, chemical reactions, etc.

## 2. Mathematical formulation

Assume the thermophoretic migration of a circular cylinder of radius $a$ having thermal conductivity $k_p$. This cylinder is embedded in a micropolar fluid, saturated with a porous medium characterized by an overall thermal conductivity $k_A$. Let $(\rho, \theta, z)$ be a system of cylindrical coordinates with origin $O$ situated at the center of the cylinder and $(\vec{e}_\rho, \vec{e}_\theta, \vec{e}_z)$ as the corresponding unit vectors. An uniform thermal gradient $\nabla T_\infty = -E_\infty \vec{e}_x$ is established far from the particle. Let $U$ denote the uniform velocity of the cylinder normal to its axis, which needs to be determined (as presented in Fig. 1). The following assumptions are considered to the study:

- The micropolar fluid flow through the homogenous Brinkman medium is steady and slow.
- The Reynolds number is sufficiently small; thus, the convective acceleration terms in the flow equations can be neglected.
- It is assumed that the thermal force is greater as compared to the inertial term; so, the Péclet number is small.

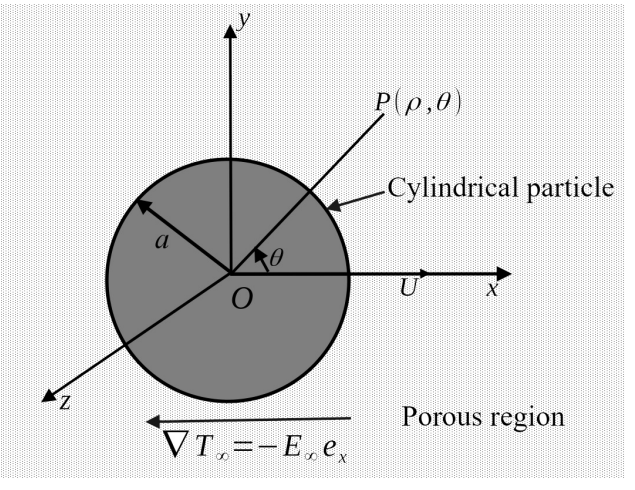


Fig. 1. Physical model of thermophoretic motion of a cylindrical particle in a micropolar fluid.

### 2.1. Governing equation in porous media

In this analysis, we utilize an equation to explain the first law of thermodynamics in porous media. We consider that the porous medium is isotropic and homogenous, leading to neglect the effects of radiation, work done by pressure changes, and the viscous dissipation terms. Consequently, the equations governing the thermal distributions for a steady state, in the absence of a heat source are [15, 21]

$$\nabla \cdot k_A \nabla T = 0, \tag{2.1}$$

where $k_A$ represents the overall thermal conductivity of the porous medium, and is

$$k_A = (1-\varphi)k_f + \varphi k_s, \tag{2.2}$$

in which $k_f$ and $k_s$ signify the thermal conductivity of fluid, thermal conductivity of solid phase of porous medium, respectively, and $\varphi$ is the porosity of the porous media.

### 2.2. Field and energy equations of micropolar fluid in porous medium

The equations, which govern the flow of micropolar fluid in a porous media in absence of inertial terms, body force and body torque are [45–47]:

$$\nabla \cdot \vec{u} = 0, \tag{2.3}$$

$$\nabla p + \frac{(\mu+\kappa_p)}{k_1}\,\vec{u} + (\mu+\kappa_p)\,\nabla \times \nabla \times \vec{u} - \kappa_p\,\nabla \times \vec{\nu} = 0, \tag{2.4}$$

$$\kappa_p \nabla \times \vec{u} - 2\,\kappa_p\,\vec{\nu} + (\alpha_0+\beta_0+\gamma_0)\,\nabla(\nabla \cdot \vec{\nu}) - \gamma_0\,\nabla \times \nabla \times\, \vec{\nu} = 0, \tag{2.5}$$

where $\vec{u}$, $p$, $\mu$, $\kappa_p$, $\vec{\nu}$, $\alpha_0$, $\beta_0$, $\gamma_0$ indicate the velocity vector, pressure, classical fluid viscosity, rotational viscosity coefficient, microrotation vector and gyroviscosity coefficients of micropolar fluid, respectively, and $k_1$ represents permeability of the porous medium.

The material coefficients ($\mu$, $\kappa_p$, $\alpha_0$, $\beta_0$, $\gamma_0$) satisfy the following inequalities:

$$\begin{aligned} &\mu \geq 0, \qquad \kappa_p \geq 0, \qquad 2\mu + \kappa_p \geq 0, \\ &\gamma_0 \geq 0, \qquad -\gamma_0 \leq \beta_0 \leq \gamma_0, \qquad 3\alpha_0 + \beta_0 + \gamma_0 \geq 0. \end{aligned}$$

The expressions for stress tensor, couple stress tensor and heat flux vector of micropolar fluid are [27, 29]:

$$\Pi = -pI + \left(\mu + \frac{\kappa_p}{2}\right)(\nabla\vec{u} + (\nabla\vec{u})^t) + \kappa_p \varepsilon \cdot (\vec{\omega} - \vec{\nu}), \tag{2.6}$$

$$\mathbf{m} = -\frac{\alpha}{\rho_A T_0}(\varepsilon \cdot \nabla T) + \alpha_0 I \cdot \nabla \vec{\nu} + \beta_0 \nabla \vec{\nu} + \gamma_0 (\nabla \vec{\nu})^t, \tag{2.7}$$

$$\vec{E} = k_A(\alpha \rho_A T_0 \nabla \times \vec{\nu} - \nabla T), \tag{2.8}$$

where $(\nabla \vec{u})^t$ represents the transpose of $\nabla \vec{u}$, also $\vec{\omega} = \frac{1}{2}\nabla \times \vec{u}$, $I$, $\varepsilon$, $\rho_A$ represent vorticity vector, unit dyadic, unit triadic, mass density, and Fourier heat conduction coefficients, respectively. $T_0$ denotes the temperature at the center of a particle, and $\alpha$ represents heat conduction due to microrotation of the micropolar fluid.

### 2.3. Boundary conditions

The first slip component, is known as a viscous slip or frictional slip, and it can be expressed mathematically for micropolar fluid

$$\vec{u}_1 = \frac{2C_m l}{2\mu + \kappa_p}(I - \vec{n}\vec{n}) \cdot (\vec{n} : \Pi), \tag{2.9}$$

where $\vec{n}$ denotes the unit normal vector at the solid surface, the quantity $C_m$ is a dimensionless quantity, known as the viscous (frictional) slip coefficient. This coefficient is related to the momentum accommodation coefficient at the solid surface, can be consider in gas rarefaction; $l$ represents the mean free path of a gaseous molecule.

The second slip component, is known as a thermal creep. For micropolar fluid, it can be given as

$$\vec{u}_2 = -\frac{C_s(2\mu + \kappa_p)}{2\rho_A T_0 k_A}(I - \vec{n}\vec{n}) \cdot \vec{E}, \tag{2.10}$$

where $C_s$ denotes the thermal creep coefficient. The velocity slip indicates thermal creep flow resulting from the longitudinal temperature gradient on the particle's surface. The thermal creep phenomenon can be included in the computations of gas flows in vacuum systems, microchannels, and several other applications where thermal imbalance leads to the gas flow.

The third velocity slip component is known as a thermal stress slip; its general form in micropolar fluid is

$$\vec{u}_3 = \frac{C_m l C_h(2\mu + \kappa_p)}{2\rho_A T_0 k_A}(I - \vec{n}\vec{n}) \cdot (\vec{n} \cdot \nabla \vec{E}), \tag{2.11}$$

where $C_h$ is the dimensionless thermal stress slip coefficient.

Additionally, the microrotation slip condition at the solid surface in a micropolar fluid is

$$\vec{\nu} = \frac{C_n l}{2\gamma_0 + \beta_0}(I - \vec{n}\vec{n}) \cdot (\vec{n} : \mathbf{m}), \tag{2.12}$$

where $C_n$ is the dimensionless spin slip coefficient.

Further, velocity and microrotation vectors vanish far away from the particle as:

$$\vec{u} \to 0, \quad \vec{\nu} \to 0, \quad \text{as } \rho \to \infty. \tag{2.13}$$

Consider the micropolar fluid flow through a porous medium is governed by (2.3)–(2.5). The velocity vector is assumed to be independent of the $z$-coordinate, therefore the velocity and microrotation vectors are:

$$\vec{u} = u_\rho(\rho,\theta)\vec{e}_\rho + u_\theta(\rho,\theta)\vec{e}_\theta, \quad \vec{\nu} = \nu_z(\rho,\theta)\vec{e}_z,$$

where $(\vec{e}_\rho, \vec{e}_\theta, \vec{e}_z)$ represent unit vectors corresponding to the directions of $\rho$, $\theta$, and $z$, respectively. The micropolar fluid flow around the particle, expressed in cylindrical polar coordinates is related to the stream function $\psi$ through

$$\vec{u} = (u_\rho, u_\theta) = \left(\frac{1}{\rho}\frac{\partial\psi}{\partial\theta}, -\frac{\partial\psi}{\partial\rho}\right). \tag{2.14}$$

Defining nondimensional parameters $\rho = a\tilde{\rho}$, $u = \tilde{u}U$, $p = (\mu U\tilde{p}/a)$, $\nabla = (\tilde{\nabla}/a)$, $\nu_z = (U\,\tilde{\nu}_z/a)$ into Eqs. (2.3)–(2.5) and eliminating the tildes, we have found the simplified equations:

$$\frac{\partial p}{\partial\rho} = -\frac{(1+\chi)}{\rho}\eta^2\frac{\partial\psi}{\partial\theta} + \frac{\chi}{\rho}\frac{\partial\nu_z}{\partial\theta} + \frac{(1+\chi)}{\rho}\frac{\partial}{\partial\theta}\nabla^2\psi, \tag{2.15}$$

$$\frac{1}{\rho}\frac{\partial p}{\partial\theta} = (1+\chi)\eta^2\frac{\partial\psi}{\partial\rho} - \chi\frac{\partial\nu_z}{\partial\rho} - (1+\chi)\frac{\partial}{\partial\rho}\nabla^2\psi, \tag{2.16}$$

$$2\nu_z + \nabla^2\psi - \frac{1}{n^2}\nabla^2\nu_z = 0, \tag{2.17}$$

where

$$\nabla^2 = \frac{\partial^2}{\partial\rho^2} + \frac{1}{\rho}\frac{\partial}{\partial\rho} + \frac{1}{\rho^2}\frac{\partial^2}{\partial\theta^2}$$

is the Laplacian operator, and various parameters in Eqs. (2.15)–(2.17) are shown in Table 1.

TABLE 1. Various non-dimensional parameters.

| Parameters | Symbols | Definition |
|---|---|---|
| Permeability parameter | $\eta$ | $\frac{a}{\sqrt{k_1}}$ |
| Micropolarity parameter | $\chi$ | $\frac{\kappa_p}{\mu}$ |
| Ratio of rotational and gyroviscosity coefficient | $n^2$ | $\frac{\kappa_p\, a^2}{\gamma_0}$ |

Eliminating pressure from Eqs. (2.15) and (2.16), we get

$$\nabla^2 \nu_z = \frac{1+\chi}{\chi}(\eta^2 \nabla^2 - \nabla^4)\psi, \tag{2.18}$$

and substitututing in Eq. (2.17),

$$\nu_z = -\frac{1}{2}\big((1-\eta^2 M)\nabla^2 \psi + M\nabla^4 \psi\big), \tag{2.19}$$

where $M = \frac{1+\chi}{\chi n^2}$.

From Eqs. (2.18) and (2.19), we get

$$\nabla^2(\nabla^2 - \lambda_1^2)(\nabla^2 - \lambda_2^2)\psi = 0, \tag{2.20}$$

where

$$\lambda_1^2 + \lambda_2^2 = 2n^2 - M^{-1} + \eta^2, \quad \lambda_1^2 \lambda_2^2 = 2\eta^2 n^2, \tag{2.21}$$

and

$$\lambda_1 = \sqrt{\frac{\eta^2 + 2n^2 - M^{-1} + \sqrt{(\eta^2 + 2n^2 - M^{-1})^2 - 8\eta^2 n^2}}{2}}, \quad \lambda_2 = \sqrt{\frac{2n^2\eta^2}{\lambda_1^2}},$$

where $\lambda_1$ and $\lambda_2$ are parameters, which depend on permeability, classical fluid viscosity, and rotational viscosity and gyroviscosities.

The solution of the sixth order partial differential equation (2.20) is given as [46]

$$\psi = \left(\frac{A}{\rho} + B\rho + CK_1(\lambda_1\rho) + DI_1(\lambda_1\rho) + EK_1(\lambda_2\rho) + FI_1(\lambda_2\rho)\right)\sin\theta, \tag{2.22}$$

by substituting the stream function in Eq. (2.19), we have found the expression for the microrotation vector

$$\nu_z = -\frac{1}{2}\big(C\xi_1 K_1(\lambda_1\rho) + D\xi_1 I_1(\lambda_1\rho) + E\xi_2 K_1(\lambda_2\rho) + F\xi_2 I_1(\lambda_2\rho)\big)\sin\theta, \tag{2.23}$$

where

$$\xi_1 = (1 - M\eta^2)\lambda_1^2 + M\lambda_1^4, \quad \xi_2 = (1 - M\eta^2)\lambda_2^2 + M\lambda_2^4,$$

and $I_n(\cdot)$, $K_n(\cdot)$ are the modified Bessel functions of the first and second kind of order $n$, respectively; $n = 0$ or 1. $A$, $B$, $C$, $D$, $E$, $F$ are arbitrary constants which will be found using boundary conditions at the particle surface. Note that, Eqs. (2.22) and (2.23), are bounded as $\rho \to \infty$ (Eq. (2.13)). So, the constants

$B, D, F \to 0$, and the stream function and microrotation vector are then given by:

$$\psi = \left(\frac{A}{\rho} + CK_1(\lambda_1\rho) + EK_1(\lambda_2\rho)\right)\sin\theta, \tag{2.24}$$

$$\nu_z = -\frac{1}{2}\big(C\xi_1 K_1(\lambda_1\rho) + E\xi_2 K_1(\lambda_2\rho)\big)\sin\theta. \tag{2.25}$$

The expression for pressure is

$$p = (1+\chi)\eta^2 A\rho^{-1}\cos\theta + \text{constant}. \tag{2.26}$$

The expressions of velocity components $u_\rho$ and $u_\theta$, normal stress $\Pi_{\rho\rho}$, shear stress $\Pi_{\rho\theta}$ and couple stress $m_{\rho z}$ are given as:

$$u_\rho = \left(\frac{A}{\rho^2} + \frac{CK_1(\lambda_1\rho)}{\rho} + \frac{EK_1(\lambda_2\rho)}{\rho}\right)\cos\theta, \tag{2.27}$$

$$u_\theta = \left[\frac{A}{\rho^2} + \frac{C}{\rho}\big(\lambda_1\rho K_0(\lambda_1\rho) + K_1(\lambda_1\rho)\big) + \frac{E}{\rho}\big(\lambda_2\rho K_0(\lambda_2\rho) + K_1(\lambda_2\rho)\big)\right]\sin\theta, \tag{2.28}$$

$$\Pi_{\rho\rho} = -(2\mu+\kappa_p)\left[\frac{A}{\rho^3}(2+\Delta_1\eta^2 r^2) + \frac{C}{\rho^2}\big(2K_1(\lambda_1\rho) + \lambda_1\rho K_0(\lambda_1\rho)\big) + \frac{E}{\rho^2}\big(2K_1(\lambda_2\rho) + \lambda_2\rho K_0(\lambda_2\rho)\big)\right]\cos\theta, \tag{2.29}$$

$$\begin{aligned}\Pi_{\rho\theta} = -(2\mu+\kappa_p)\Bigg[&\frac{2A}{\rho^3} + \frac{C}{\rho^2}\Big(K_1(\lambda_1\rho)\Big(\frac{\lambda_1^2\rho^2}{2}+2\Big) + \lambda_1\rho K_0(\lambda_1\rho)\Big)\\ &+ \frac{E}{\rho^2}\Big(K_1(\lambda_2\rho)\Big(\frac{\lambda_2^2\rho^2}{2}+2\Big) + \lambda_2\rho K_0(\lambda_2\rho)\Big)\\ &- \frac{\kappa_p}{2(2\mu+\kappa_p)}\big(CK_1(\lambda_1\rho)(\xi_1-\lambda_1^2) + EK_1(\lambda_2\rho)(\xi_2-\lambda_2^2)\big)\Bigg]\sin\theta,\end{aligned} \tag{2.30}$$

$$\begin{aligned}m_{\rho z} = \Bigg[&\frac{(2\gamma_0+\beta_0)}{2\rho}\big(C\xi_1 K_1(\lambda_1\rho) + E\xi_2 K_1(\lambda_2\rho)\big)\\ &+ \frac{\gamma_0}{2\rho}\Big(C\xi_1(\lambda_1\rho K_0(\lambda_1\rho) - K_1(\lambda_1\rho))\\ &+ E\xi_2\big(\lambda_2\rho K_0(\lambda_2\rho) - K_1(\lambda_2\rho)\big)\Big) + 2\alpha Z\left(1 - \frac{B_1}{\rho^2}\right)\Bigg]\sin\theta,\end{aligned} \tag{2.31}$$

where

$$\Delta_1 = \frac{\mu+\kappa_p}{2\mu+\kappa_p}.$$

**2.4. Temperature distributions**

The governing equations of the temperature inside a cylindrical particle and for the micropolar fluid are governed by the Laplace equation as follows:

$$\nabla^2 T_p = 0, \qquad \rho < a, \tag{2.32}$$

$$\nabla^2 T = 0, \qquad \rho > a. \tag{2.33}$$

The convective heat transfer term is not included in Eqs. (2.32) and (2.33). The Reynolds number and Péclet number are very small for the present study of slow micropolar fluid flow. The heat flux vector of micropolar fluid ($\vec{E}$) and the particle ($\vec{E_p}$) are defined as [29, 30]:

$$\vec{E} = k_A(\alpha\rho_A T_0 \nabla \times \vec{\nu} - \nabla T), \tag{2.34}$$

$$\vec{E_p} = -k_p \nabla T_p. \tag{2.35}$$

**Temperature jump and heat flux continuous conditions**

At the particle surface $\rho = a$, we assume the temperature jump condition and contnuity of heat flux:

$$T - T_p = -\frac{C_t l}{k_A}(\vec{E} \cdot \vec{e_\rho}), \tag{2.36}$$

$$\vec{E} \cdot \vec{e_\rho} = \vec{E_p} \cdot \vec{e_\rho}, \tag{2.37}$$

with

$$T \to T_\infty = T_0 - E_\infty \rho \cos\theta, \qquad \text{as } \rho \to \infty, \tag{2.38}$$

where $C_t$ denotes the temperature jump coefficient at the particle surface.

Applying the boundary conditions (2.36)–(2.38) in Eqs. (2.32)–(2.33), we get following systems of linear equations:

$$A_1 - B_1(1 + \tilde{C_t})a^{-2} = \tilde{C_t} - 1 - \frac{\tilde{C_t}\alpha}{2aZ}(C\xi_1 K_1(\lambda_1 a) + E\xi_2 K_1(\lambda_2 a)), \tag{2.39}$$

$$kA_1 + B_1 a^{-2} = \frac{\alpha}{2aZ}(C\xi_1 K_1(\lambda_1 a) + E\xi_2 K_1(\lambda_2 a)) - 1. \tag{2.40}$$

Temperature distributions within and outside the particle are given as:

$$T_p = T_0 + A_1 E_\infty \rho \cos\theta, \tag{2.41}$$

$$T = T_0 - E_\infty(1 + B_1\rho^{-2})\rho\cos\theta, \tag{2.42}$$

where

$$A_1 = -2\delta_1 + \frac{\alpha(C\xi_1 K_1(\lambda_1 a) + E\xi_2 K_1(\lambda_2 a))}{2Z},$$
$$B_1 = -\delta_1\delta_2 + \frac{\alpha\delta_1\delta_3(C\xi_1 K_1(\lambda_1 a) + E\xi_2 K_1(\lambda_2 a))}{2Z},$$
$$\delta_1 = (1 + k(\tilde{C}_t + 1))^{-1}, \quad \delta_2 = (1 + k(\tilde{C}_t - 1)), \quad \delta_3 = (1 + k\tilde{C}_t),$$
$$\tilde{C}_t = \frac{C_t l}{a}, \quad k = \frac{k_p}{k_A}, \quad Z = \frac{E_\infty}{\rho_A T_0}.$$

### 2.5. Slip conditions at the particle surface

At the cylindrical particle surface, boundary conditions are as follows [30]:

$$u_\rho = U\cos\theta, \tag{2.43}$$

$$u_\theta = -U\sin\theta + \frac{2C_m l}{2\mu + \kappa_p}\Pi_{\rho\theta} + \frac{C_s(2\mu + \kappa_p)}{2}\left(\frac{1}{\rho_A T_0 \rho}\frac{\partial T}{\partial\theta} + \frac{\alpha}{\rho}\frac{\partial}{\partial\rho}(\rho\nu_z)\right) - \frac{C_m l C_h(2\mu + \kappa_p)}{2}\left(\frac{1}{\rho_A T_0}\frac{\partial}{\partial\rho}\left(\frac{1}{\rho}\frac{\partial T}{\partial\theta}\right) + \alpha\frac{\partial}{\partial\rho}\left(\frac{1}{\rho}\frac{\partial}{\partial\rho}(\rho\nu_z)\right)\right), \tag{2.44}$$

$$\nu_z = \frac{C_n l}{2\gamma_0 + \beta_0} m_{\rho z}. \tag{2.45}$$

The conditions far away from the particle are:

$$u_\rho = u_\theta = \nu_z = 0, \quad \text{as } \rho \to \infty. \tag{2.46}$$

Putting the expressions from Eqs. (2.27)–(2.31) into the boundary conditions (2.43)–(2.45), we get a set of linear equations for finding the unknowns $A$, $C$, and $E$:

$$A + CS_1 + ES_2 = U, \tag{2.47}$$

$$2A\Upsilon_1 + 2C(S_1 + \lambda_1 S_3 + \tilde{C}_m\Upsilon_3 - \tilde{C}_m C_h\Upsilon_2\Upsilon_8 - C_s\Upsilon_4\Upsilon_8) + 2E(S_2 + \lambda_2 S_4 + \tilde{C}_m\Upsilon_6 - \tilde{C}_m C_h\Upsilon_5\Upsilon_8 - C_s\Upsilon_7\Upsilon_8) + 2U = (C_s - H_1 B_1)\Upsilon_8 Z, \tag{2.48}$$

$$H_2 Z B_1 + C\Upsilon_9 + E\Upsilon_{10} = H_2 Z, \tag{2.49}$$

where

$$\tilde{\gamma_0} = \frac{\gamma_0}{2\gamma_0 + \beta_0}, \quad \tilde{C_m} = \frac{C_m l}{a}, \quad \tilde{C}_n = \frac{C_n l}{a},$$

and $S_i$, $i = 1$ to 4, $\Upsilon_j$, $j = 1$ to 10, $H_1$, $H_2$ are shown in Appendix.

**2.6. Thermophoretic velocity and force**

The drag force exerted on the cylindrical particle embedded in a micropolar fluid is given as

$$F = \int_0^{2\pi} [\rho(\Pi_{\rho\rho}\cos\theta - \Pi_{\rho\theta}\sin\theta)]_{\rho=1}\, d\theta. \tag{2.50}$$

Substituting $\Pi_{\rho\rho}$ and $\Pi_{\rho\theta}$ in Eq. (2.50), we get an expression for the drag force

$$F = -\pi\left(A\zeta_5 - CS_1\zeta_6 - ES_2\zeta_7\right). \tag{2.51}$$

Since the cylindrical particle remains suspended freely in the micropolar fluid, the drag force $F$ must vanish under a thermal gradient. Hence

$$A\zeta_5 - CS_1\zeta_6 - ES_2\zeta_7 = 0. \tag{2.52}$$

Using Eq. (2.52), we get the thermophoretic velocity of the cylindrical particle, which is:

$$U_T = Z\frac{\zeta_{69} + \zeta_{70} + \zeta_{71} + \zeta_{72} + \zeta_{73} + \zeta_{74} + \zeta_{75}}{\zeta_{76} + \zeta_{77} + \zeta_{78} + \zeta_{79} + \zeta_{80} + \zeta_{81}}. \tag{2.53}$$

Also by substituting $U_T = 0$ in Eq. (2.51), we get the thermophoretic force given as:

$$F_T = Z\pi\frac{\zeta_{69} + \zeta_{70} + \zeta_{71} + \zeta_{72} + \zeta_{73} + \zeta_{74} + \zeta_{75}}{\zeta_{82} + \zeta_{83} + \zeta_{84} + \zeta_{85} + \zeta_{86} + \zeta_{87}}. \tag{2.54}$$

The expressions for normalized thermophoretic velocity and force are defined as:

$$U_T^* = \frac{U_T}{\mu(1+\chi)C_sZ}, \tag{2.55}$$

$$F_T^* = \frac{lF_T}{\mu^2a^2(1+\chi)^2Z}, \tag{2.56}$$

where $S_i$, $i = 1$ to 6, and $\zeta_m$, $m = 1$ to 87 are presented in Appendix.

**Some specific cases**

**Case I**: When a medium is the porous medium saturated viscous fluid. If $\chi \to 0$, i.e., ($\kappa_p \to 0$, $\lambda_1 \to \eta$, $\lambda_2 \to \infty$), the thermophoretic velocity and force are given as:

$$U_T = 4\mu Z \frac{S_5(C_s\delta_3 + \tilde{C_m}C_h\delta_2)\delta_1}{((1+2\tilde{C_m})\eta S_6 + (\tilde{C_m}\eta^2 + 4(1+2\tilde{C_m}))S_5)}, \tag{2.57}$$

$$F_T = \pi\mu U_T\eta^2 \frac{((1+2\tilde{C_m})\eta S_6 + (\tilde{C_m}\eta^2 + 4(1+2\tilde{C_m}))S_5)}{(1+2\tilde{C_m})\eta S_6 + \tilde{C_m}\eta^2 S_5)}. \tag{2.58}$$

These results agree with the results of FALTAS and RAGAB [21].

**Case II**: When the particle embedded in the Newtonian fluid, *i.e.*, $k_1 \to \infty$, and $\chi \to 0$, Eqs. (2.57) and (2.58) reduce to:

$$U_T = \mu Z \frac{(C_s\delta_3 + \tilde{C_m}C_h\delta_2)\delta_1}{C_s(1+2\tilde{C_m})}, \tag{2.59}$$

$$F_T = \pi\mu U_T \frac{C_s(1+2\tilde{C_m})}{\tilde{C_m}}. \tag{2.60}$$

The above results are matches with the work of CHANG and KEH [10].

**Subcase I**: When the thermal stress slip parameter vanishes, i.e., $C_h \to 0$, Eqs. (2.59)–(2.60) transform to:

$$U_T = \mu Z \frac{C_s\delta_3\delta_1}{C_s(1+2\tilde{C_m})}, \tag{2.61}$$

$$F_T = \pi\mu U_T \frac{C_s(1+2\tilde{C_m})}{\tilde{C_m}}. \tag{2.62}$$

The expressions are the same as the results of KEH and TU [9].

## 3. Numerical results and their analysis

This study presents the thermophoretic movement of a solid cylinder within a porous medium composed of micropolar fluid. In this study, we have derived explicit expressions for thermal distributions, thermophoretic velocity, and thermophoretic force. In this section, we visualize the effects of several parameters, such as micropolarity, permeability, thermal conductivity, and slip parameters, on thermophoretic velocity and force. In our analysis, we utilized the available data for several coefficients: thermal jump ($C_t = 2.18$), frictional slip ($C_m = 1.14$), thermal creep ($C_s = 1.17$), spin slip ($C_n = 1.2$), and gyroviscosity coefficients ($\gamma_0/\mu a^2 = 0.3$, $\beta_0/\mu a^2 = 0.2$) [46, 49].

The variation of the thermophoretic velocity and thermophoretic force is shown graphically in Figs. 2–15 with the following parameters:

1. Knudsen number ($0.01 \leq K_n \leq 1$) [20, 21].
2. Thermal conductivity ratio ($0 < k < \infty$) [20, 21].

3. Micropolarity parameter ($0 \leq \chi < \infty$) [29].
4. Permeability ($0 < k_1 < \infty$) [20, 48].
5. Frictional slip parameter ($0 \leq \tilde{C_m} < \infty$) [29, 48].
6. Thermal stress slip parameter ($0 \leq C_h < \infty$) [21].
7. Microrotation thermal conductivity parameter ($0 \leq \alpha\mu/a^2 < \infty$) [29].
8. Thermal jump parameter ($0 \leq \tilde{C_t} < \infty$).

### 3.1. Thermophoretic velocity

The thermophoretic velocity indicates the motion of a particle from hot regions to cold regions, suspended in a fluid under the impact of a thermal gradient.

Figure 2 illustrates the variation of the normalized thermophoretic velocity $U_T^*$ versus the Knudsen number for different values of the thermal conductivity ratio and micropolarity parameters. Generally, the graph shows that $U_T^*$ decreases steadily as the Knudsen number increases. Additionally, the thermophoretic velocity declines with an rise in the thermal conductivity ratio. This mechanism occurs because a higher thermal conductivity of the particle reduces the local temperature gradient at its surface. For various values of the Knudsen number $K_n$ and the thermal conductivity ratio $k$, the thermophoretic velocity decreases as the micropolarity parameter increases. This reduction is due to the fact that the thickness of a micropolar fluid is higher than that of the Newtonian fluid, leading to a decrease in particle velocity.

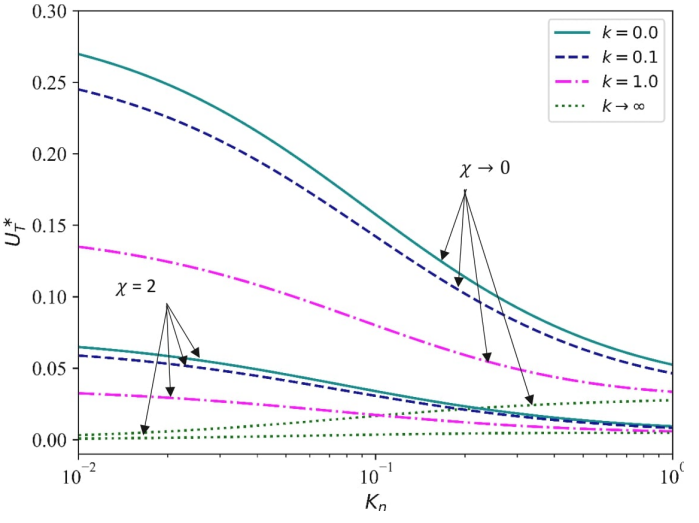


FIG. 2. Variation of $U_T^*$ versus $K_n$ when $\alpha\mu/a^2 = 0.2$, $C_h = 1$, $k_1 = 0.01$.

Figure 3 shows the influence of increasing viscous slip and thermal stress slip parameters on the thermophoretic velocity versus the Knudsen number.

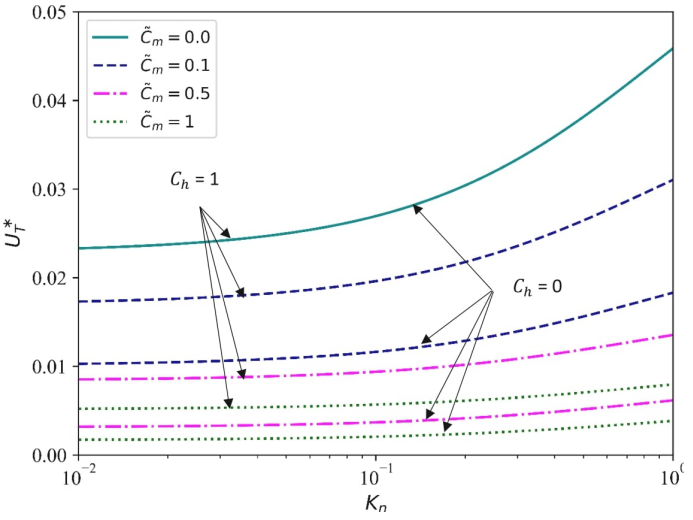


FIG. 3. Variation of $U_T^*$ versus $K_n$ when $k = 1$, $\chi = 3$, $\alpha\mu/a^2 = 0.2$, $k_1 = 0.01$.

The graph reveals that the thermophoretic velocity reduces as the frictional slip parameter enhances, while it tends to increase with a rise in the thermal stress slip parameter. Notably, the effect of the thermal stress slip parameter on velocity remains consistent, when the frictional slip parameter is zero.

Figure 4 reveals the relationship between the thermophoretic velocity and the micropolarity parameter for numerous values of the Knudsen number and the thermal stress slip parameter. As depicted, the velocity consistently

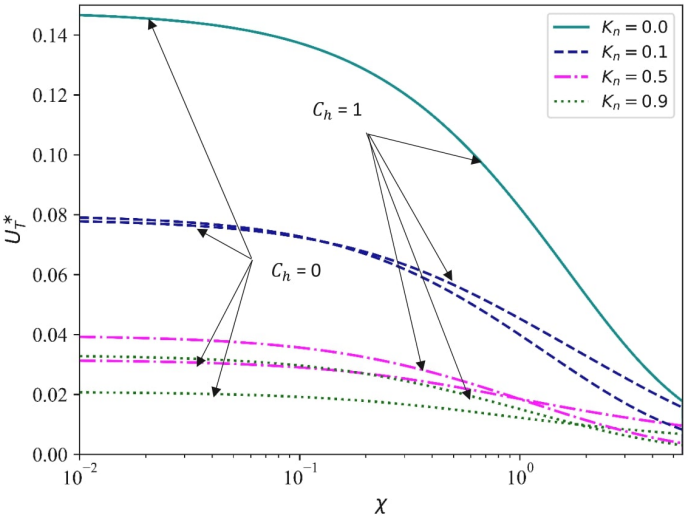


FIG. 4. Variation of $U_T^*$ versus $\chi$ when $k = 1$, $\alpha\mu/a^2 = 0.1$, $k_1 = 0.01$.

decreases with a rise in the micropolarity parameter, while the other parameters are held constant. This reduction occurs because the increasing thickness of the medium reduces thermophoretic mobility. Additionally, the plots show that $U_T^*$ decreases as the Knudsen number increases. The influence of the thermal stress slip parameter on the thermophoretic velocity is also evident in this graph, indicating that there is no effect on the velocity when the Knudsen number approaches to zero.

The variation of thermophoretic velocity versus the Knudsen number is presented in Fig. 5. As the thermal conductivity ratio increases (indicating a rise in the particle thermal conductivity), the normalized velocity decreases in the entire range of the Knudsen number. This happens because higher thermal conductivity of the particle reduces the local temperature gradient at its surface. However, for the case where the thermal conductivity ratio becomes very large, we see that the thermophoretic velocity increases with the Knudsen number. In this graph, it is also interesting to note that the thermophoretic velocity decreases for a higher microrotation thermal conductivity parameter.

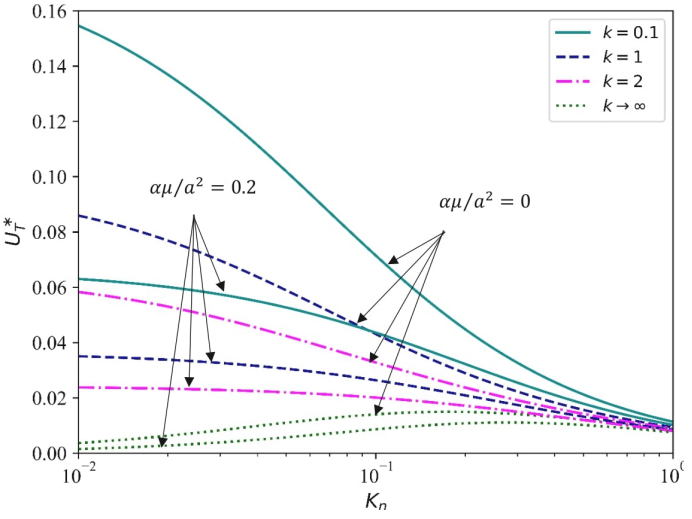


Fig. 5. Variation of $U_T^*$ versus $K_n$ when $C_h = 0$, $\chi = 2$, $k_1 = 0.01$.

Figures 6–9 illustrate the variation of thermophoretic velocity versus permeability for different parameters, including the thermal conductivity ratio, viscous slip parameter, Knudsen number, and temperature jump parameter. Figure 6 shows that thermophoretic velocity increases with higher permeability. Lower permeability indicates that frictional forces dominate over inertial forces, suggesting that the medium is more porous. Conversely, higher permeability means that inertial forces dominate, indicating a clear fluid. Thus, as perme-

ability rises, the thermophoretic velocity also increases. Additionally, it is important to note that as the thermal conductivity ratio increases, the thermophoretic velocity decreases. The reason for the consequence is explained earlier. Figure 7 depicts the impact of the frictional slip parameter on the thermophoretic velocity. The graph demonstrates that the velocity $U_T^*$ rises as the frictional slip parameter decreases. A reduction in the slip parameter leads to an increase in the

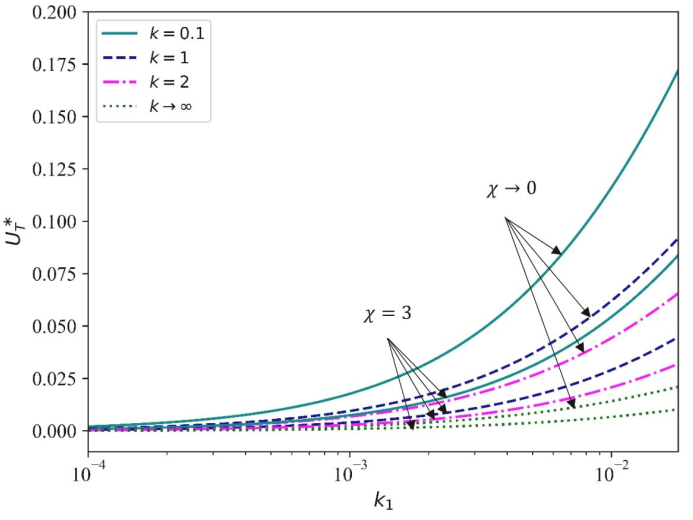


FIG. 6. Variation of $U_T^*$ versus $k_1$ when $K_n = 0.2$, $C_h = 2$, $\alpha\mu/a^2 = 0$.

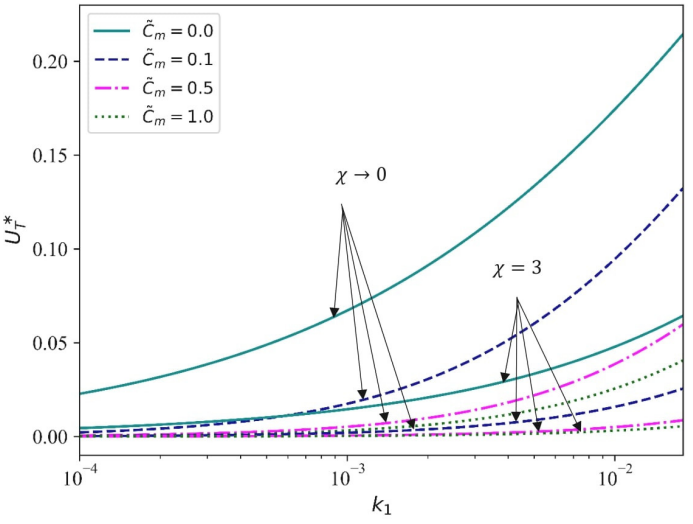


FIG. 7. Variation of $U_T^*$ versus $k_1$ when $k = 1$, $K_n = 0.2$, $C_h = 2$, $\alpha\mu/a^2 = 0.1$.

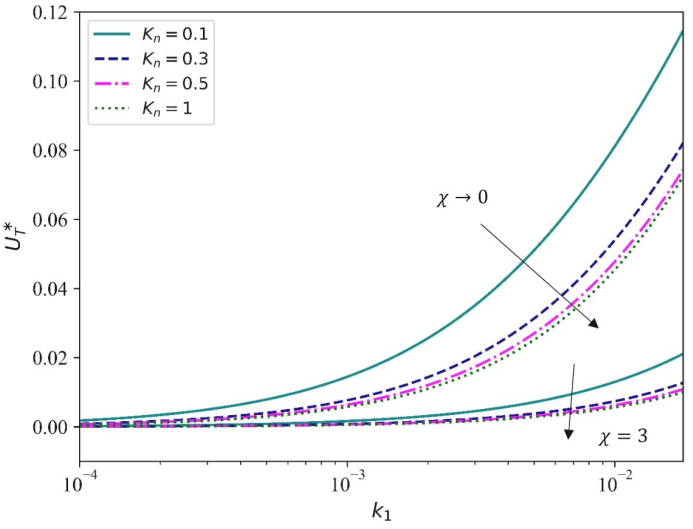


FIG. 8. Variation of $U_T^*$ versus $k_1$ when $C_h = 2$, $k = 1$, $\alpha\mu/a^2 = 0.1$.

mobility of the particles within the fluid medium. Figure 8 depicts the impact of the increasing Knudsen number on the thermophoretic velocity. The graph shows that as the Knudsen number increases, the velocity decreases. Figure 9 presents the impact of the temperature jump parameter on the thermophoretic velocity. This indicates that $U_T^*$ increases monotonically with a higher temperature jump parameter.

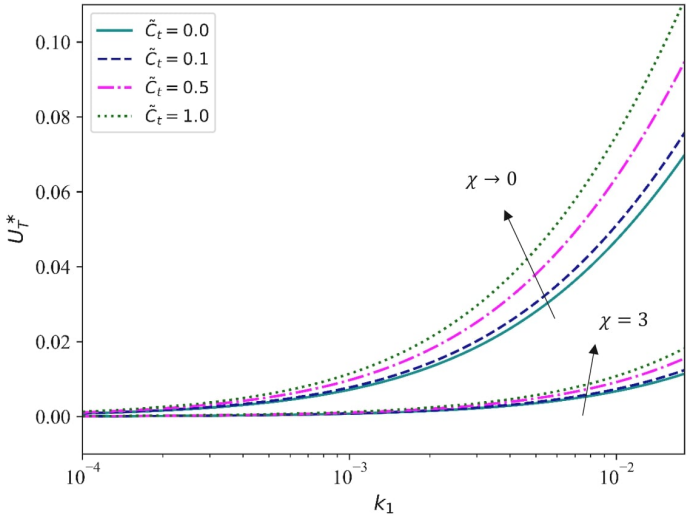


FIG. 9. Variation of $U_T^*$ versus $k_1$ when $k = 1$, $K_n = 0.2$, $C_h = 2$, $\alpha\mu/a^2 = 0.1$.

### 3.2. Thermophoretic force

The thermophoretic force arises when particles move in a fluid due to a thermal gradient. The magnitude of this force depends on the strength of the temperature gradient as well as the physical characteristics of the particles and the surrounding fluid.

The graphical representation of the normalized thermophoretic force as a function of the Knudsen number is shown in Fig. 10 for diverse values of the thermal stress slip and micropolarity parameters. The thermophoretic force consistently increases, throughout the entire range of the Knudsen number. Additionally, this force rises with an increase in the thermal stress slip parameter. It is important to note that the change in the thermophoretic force is less significant in micropolar fluids compared to viscous fluids, primarily due to the greater thickness of the micropolar fluid.

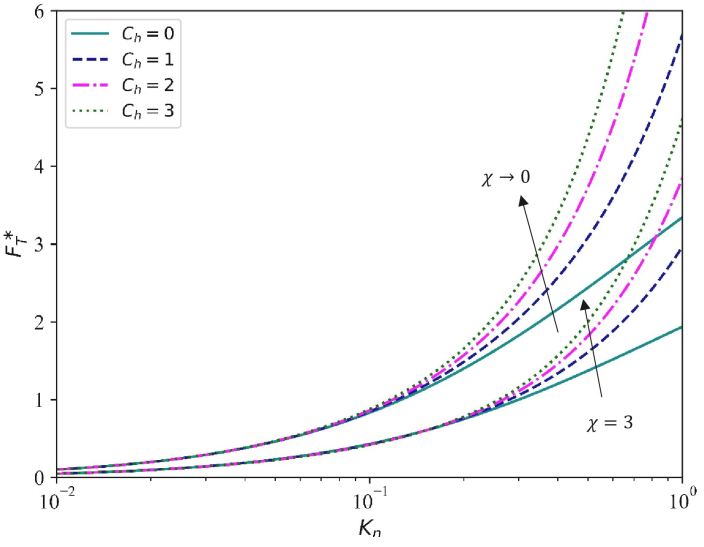


FIG. 10. Variation of $F_T^*$ versus $K_n$ when $k = 1$, $\alpha\mu/a^2 = 0.1$, $k_1 = 1$.

Figure 11 presents that the thermophoretic force decreases as the thermal conductivity ratio and micropolarity parameters increase. This trend may be explained by the fact that the higher thermal conductivity of the particle reduces the thermal gradient at its surface across various values of the Knudsen number. Additionally, we observe that the thermophoretic force declines as the Knudsen number decreases. From this graph, we can conclude that the thermophoretic force is a decreasing function of the thermal conductivity ratio and micropolarity parameters, while it is an increasing function of the Knudsen number.

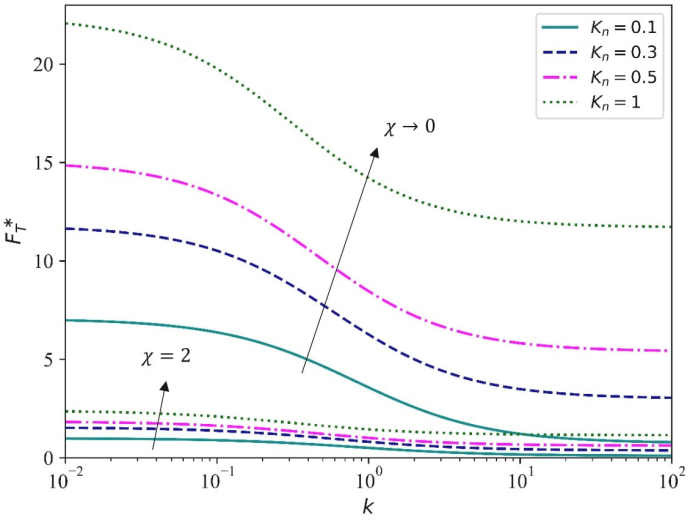


FIG. 11. Variation of $F_T^*$ versus $k$ when $C_h = 2$, $\alpha\mu/a^2 = 0.1$, $k_1 = 0.01$.

Figure 12 demonstrates that the thermophoretic force decreases across the entire range of the micropolarity parameter for various values of the viscous slip parameter and thermal conductivity ratio. A rise in the micropolarity parameter indicates more significant microstructural effects than those observed in the Newtonian fluid, leading to greater resistance for fluid flow due to microrotational viscosity. Consequently, the thermophoretic force decreases. Additionally,

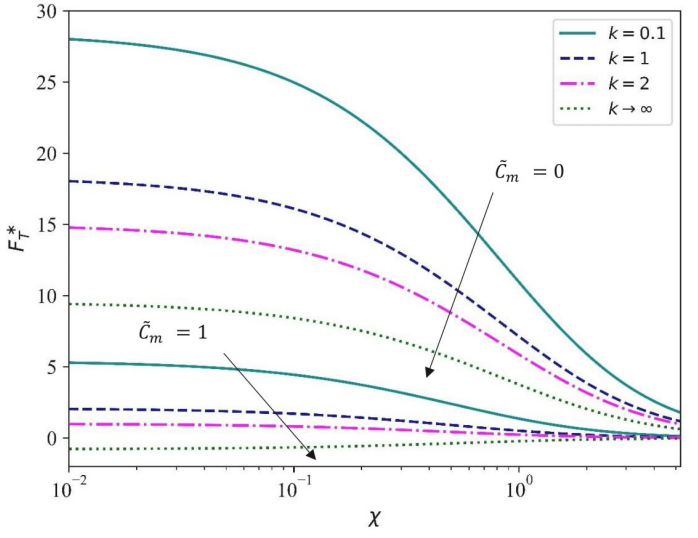


FIG. 12. Variation of $F_T^*$ versus $\chi$ when $C_h = 0$, $K_n = 0.2$, $\alpha\mu/a^2 = 0.2$, $k_1 = 0.01$.

it is observed that the thermophoretic force is a decreasing function of both the frictional slip parameter and thermal conductivity ratio.

Figures 13–15 represent the variation of the thermophoretic force versus the permeability for different parameters such as the thermal conductivity ratio, frictional slip parameter, and Knudsen number. From these figures, we observe that as permeability increases, the thermophoretic force decreases. Figure 13

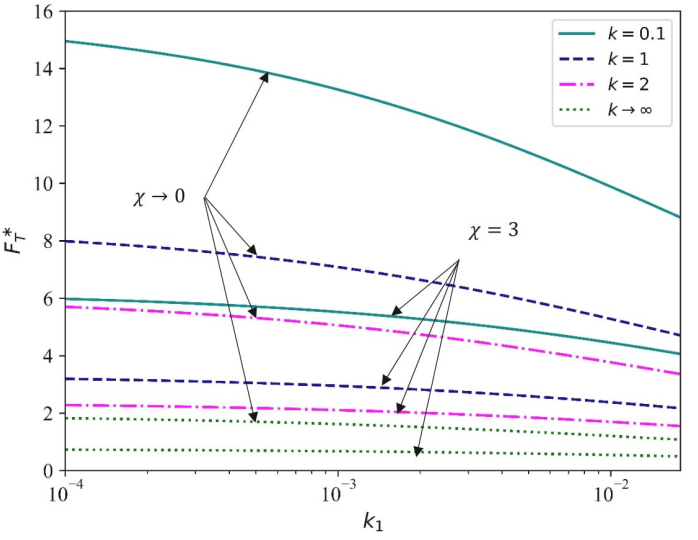


FIG. 13. Variation of $F_T^*$ versus $k_1$ when $K_n = 0.2$, $C_h = 2$, $\alpha\mu/a^2 = 0$.

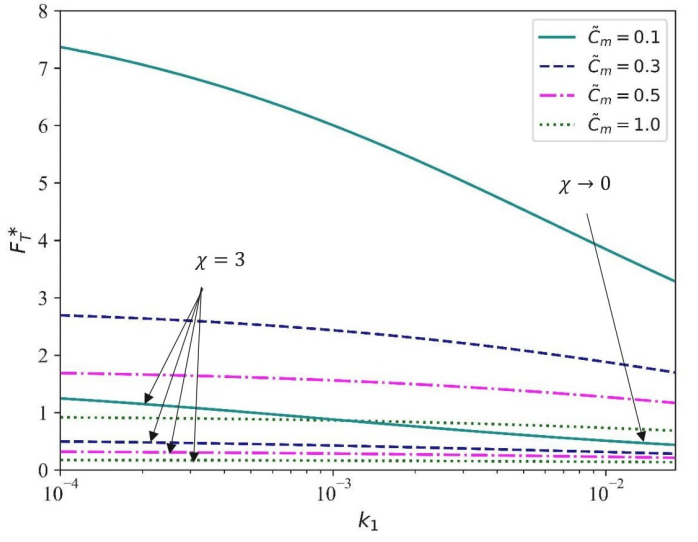


FIG. 14. Variation of $F_T^*$ versus $k_1$ when $k = 1$, $K_n = 0.2$, $C_h = 2$, $\alpha\mu/a^2 = 0.1$.

shows the impact of the thermal conductivity ratio on the thermophoretic force, showing a decline in the force as the thermal conductivity ratio increases. In Fig. 14, the variation of the thermophoretic force with respect to the permeability is presented. The graph illustrates that the thermophoretic force decreases as the frictional slip parameter increases. Significantly, the force is greatest when the frictional slip parameter is low. A graphical representation of the force versus permeability is shown in Fig. 15. This graph shows that the thermophoretic force increases as the Knudsen number increases.

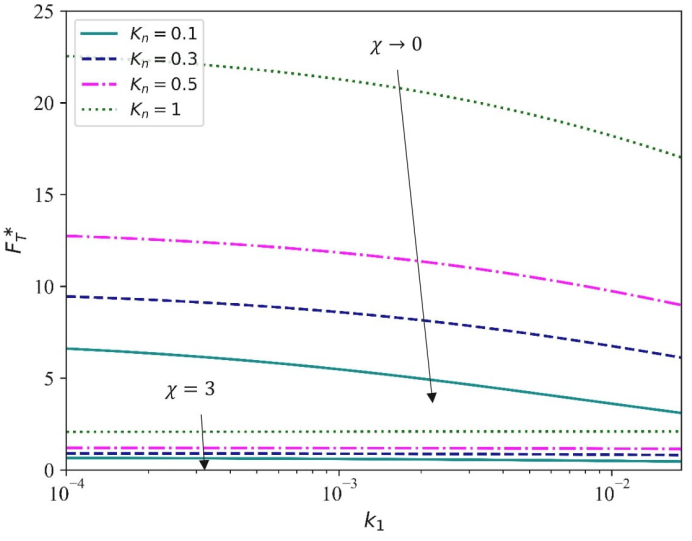


Fig. 15. Variation of $F_T^*$ versus $k_1$ when $k = 1$, $C_h = 2$, $\alpha\mu/a^2 = 0.1$.

## 4. Conclusions

In this study, we investigate the migration of a cylindrical particle normal to its axis in micropolar porous media under a uniform temperature gradient. The governing equations for fluid motion and heat transfer in this two-dimensional problem are solved analytically, accounting for thermal jump, heat flux continuity, viscous slip, thermal creep, thermal stress slip, and microrotation slip conditions. The thermophoretic velocity and force have been calculated for various values of the Knudsen number, permeability, micropolarity parameter, thermal conductivity ratio of the particle to the medium, microrotation thermal conductivity parameter, and hydrodynamic slip parameters. It is observed that both the thermophoretic velocity and the force decrease as the micropolarity parameter and microrotation thermal conductivity parameter increase. Additionally, the thermophoretic velocity increases with higher permeability, while the ther-

mophoretic force decreases with both higher permeability and thermal conductivity of the particle. Furthermore, it is noted that the thermophoretic velocity and force exhibit greater variation when the thermal stress slip parameter is non-zero, and the frictional slip parameter is zero.

Our findings indicate a well agreement with previously published results regarding Brinkman media and viscous fluids (with and without thermal stress slip). The problems of thermophoretic motion of circular solid cylinders are fundamental in many scientific and engineering sectors, such as fouling of combustion engine walls, modified chemical vapour deposition process, gas filtration, and electromagnetic chip production. Considering thermophoretic motion of various geometries such as deformed sphere, deformed cylinder, and spheroid in an unbounded micropolar fluid through an isotropic porous medium undergoing chemical reaction, Brownian motion, photophoresis and magnetic effects are future aspects. Additionally, the research should be extended to investigate thermophoretic migration of aerosol particles in spherical and cylindrical cavities, as well as in microtubes filled with Brinkman micropolar fluid, couple stress fluid, and other non-Newtonian fluids with a nonuniform temperature gradient.

## Appendix

The expressions mentioned in Eqs. (2.47)–(2.49), and Eqs. (2.53)–(2.54) are:

$$
\begin{aligned}
&S_1 = K_1(\lambda_1), && S_2 = K_1(\lambda_2),\\
&S_3 = K_0(\lambda_1), && S_4 = K_0(\lambda_2),\\
&S_5 = K_1(\eta), && S_6 = K_0(\eta),\\
&H_1 = (C_s + 2\tilde{C_m}C_h), && H_2 = -\frac{2\tilde{C_n}\alpha\tilde{\gamma_0}}{\gamma_0},\\
&H_3 = (\lambda_1^2+4)S_1 + 2\lambda_1 S_3, && H_4 = \frac{\chi}{2+\chi}(\xi_1 - \lambda_1^2)S_1,\\
&H_5 = (\lambda_2^2+4)S_2 + 2\lambda_2 S_4, && H_6 = \frac{\chi}{2+\chi}(\xi_2 - \lambda_2^2)S_2,\\
&\Upsilon_1 = 1 + 4\tilde{C_m}, && \Upsilon_2 = \frac{\alpha\xi_1\lambda_1^2 S_1}{4},\\
&\Upsilon_3 = H_3 - H_4, && \Upsilon_4 = \frac{\alpha\xi_1\lambda_1 S_3}{4},\\
&\Upsilon_5 = \frac{\alpha\xi_2\lambda_2^2 S_2}{4}, && \Upsilon_6 = H_5 - H_6,\\
&\Upsilon_7 = \frac{\alpha\xi_2\lambda_2 S_4}{4}, && \Upsilon_8 = 2 + \chi,
\end{aligned}
$$

$$\Upsilon_9 = \xi_1(S_1(1+\tilde{C_n}) - \tilde{\gamma_0}\tilde{C_n}(S_1 - \lambda_1 S_3)),$$
$$\Upsilon_{10} = \xi_2(S_2(1+\tilde{C_n}) - \tilde{\gamma_0}\tilde{C_n}(S_2 - \lambda_2 S_4)),$$
$$\zeta_1 = \tilde{C_t} + 1, \qquad \zeta_2 = \tilde{C_t} - 1,$$
$$\zeta_3 = \frac{\tilde{C_t}\alpha}{2}, \qquad \zeta_4 = \frac{\alpha}{2},$$
$$\zeta_5 = (1+\chi)\eta^2, \qquad \zeta_6 = \chi\lambda_1^2 + \lambda_1^2 - \frac{\chi\xi_1}{2},$$
$$\zeta_7 = \chi\lambda_2^2 + \lambda_2^2 - \frac{\chi\xi_2}{2},$$
$$\zeta_8 = (H_1 + C_s)(k\zeta_2 + 1)\Upsilon_8\Upsilon_9(\zeta_5 + \zeta_7),$$
$$\zeta_9 = H_2 S_1 k(\zeta_2 + \zeta_1)\zeta_6\Upsilon_7\Upsilon_8,$$
$$\zeta_{10} = H_2 S_1(2\zeta_6 + k\zeta_2\zeta_5)\Upsilon_7\Upsilon_8,$$
$$\zeta_{11} = H_2 S_1(k\zeta_1 + 2)\zeta_5\Upsilon_7\Upsilon_8,$$
$$\zeta_{12} = H_2 S_1 k(\zeta_2 + \zeta_1)\zeta_6\Upsilon_5\Upsilon_8,$$
$$\zeta_{13} = H_2 S_1(2\zeta_6 + k\zeta_2\zeta_5)\Upsilon_5\Upsilon_8,$$
$$\zeta_{14} = H_2 S_1(k\zeta_1 + 2)\zeta_5\Upsilon_5\Upsilon_8,$$
$$\zeta_{15} = (k\zeta_2\zeta_7 + k\zeta_1\zeta_7 + 2\zeta_7 + k\zeta_2\zeta_5)\Upsilon_4\Upsilon_8,,$$
$$\zeta_{16} = (C_s(k\zeta_1 + 2)\zeta_5\Upsilon_4)\Upsilon_8,$$
$$\zeta_{17} = 2H_2 S_2(\zeta_2 + \zeta_1)\zeta_7\Upsilon_2\Upsilon_8,$$
$$\zeta_{18} = H_2 S_2(2\zeta_7 + k\zeta_2\zeta_5 + k\zeta_1\zeta_5 + 2\zeta_5)\Upsilon_2\Upsilon_8,$$
$$\zeta_{19} = (H_1 + S_1)(k\zeta_2 + 1)\Upsilon_{10}\Upsilon_8(\zeta_5 + \zeta_6),$$
$$\zeta_{20} = (H_1 - S_1)H_2 S_1 S_2(\zeta_4 + k\zeta_3)\Upsilon_8,$$
$$\zeta_{21} = \zeta_6\xi_2 + \zeta_5\xi_2 - \zeta_7\xi_1 - \zeta_5\xi_1,$$
$$\zeta_{22} = (k\zeta_2\zeta_6 + k\zeta_1\zeta_6 + 2\zeta_6 + k\zeta_2\zeta_5)\Upsilon_6,$$
$$\zeta_{23} = S_1(k\zeta_1 + 2)\zeta_5\Upsilon_6 - S_2 k(\zeta_2 + \zeta_1)\zeta_7\Upsilon_3,$$
$$\zeta_{24} = (2\zeta_7 + k\zeta_2\zeta_5 + k\zeta_1\zeta_5 + 2\zeta_5)\Upsilon_3,$$
$$\zeta_{25} = S_1 S_2(k\zeta_2\zeta_7 + k\zeta_1\zeta_7 + 2\zeta_7 - k\zeta_2\zeta_6)\Upsilon_1,$$
$$\zeta_{26} = S_2 k\zeta_1\Upsilon_1 + 2S_2\Upsilon_1 - S_4 k(\zeta_2 + \zeta_1)\lambda_2,$$
$$\zeta_{27} = (2\zeta_6 + k\zeta_2\zeta_5 + k\zeta_1\zeta_5 + 2\zeta_5)\lambda_2,$$
$$\zeta_{28} = (k\zeta_2\zeta_7 + k\zeta_1\zeta_7 + 2\zeta_7 + k\zeta_2\zeta_5)\lambda_1,$$
$$\zeta_{29} = S_3 k\zeta_1\zeta_5\lambda_1 + 2S_3\zeta_5\lambda_1 + S_1 k\zeta_2\zeta_7 + S_1 k\zeta_1\zeta_7,$$
$$\zeta_{30} = 2\zeta_7 - k\zeta_2\zeta_6 - k\zeta_1\zeta_6 - 2\zeta_6,$$
$$\zeta_{31} = (k\zeta_1 + 1)\zeta_5(C_s\Upsilon_7 + C_h\tilde{C_m}\Upsilon_5)\Upsilon_8\Upsilon_9,$$
$$\zeta_{32} = (\zeta_4 + k\zeta_3)\zeta_5\xi_2\Upsilon_8\Upsilon_9,$$

$$\zeta_{33} = (k\zeta_1 + 1)\zeta_5\Upsilon_6\Upsilon_9,$$
$$\zeta_{34} = (k\zeta_1 + 1)(S_2\zeta_7\Upsilon_1 + S_4\zeta_5\lambda_2)\Upsilon_9,$$
$$\zeta_{35} = (k\zeta_1 + 1)(\zeta_7 + 2\zeta_5)\Upsilon_9,$$
$$\zeta_{36} = (\zeta_4 + k\zeta_3)\zeta_5\xi_1\Upsilon_8,$$
$$\zeta_{37} = C_s\Upsilon_7 + \tilde{C}_m C_h\Upsilon_5,$$
$$\zeta_{38} = (k\zeta_1 + 1)\zeta_5\Upsilon_{10}\Upsilon_4\Upsilon_8,$$
$$\zeta_{39} = H_2S_2(\zeta_4 + k\zeta_3)\zeta_5\xi_2\Upsilon_4\Upsilon_8,$$
$$\zeta_{40} = (k\zeta_1 + 1)\zeta_5\Upsilon_{10}\Upsilon_2\Upsilon_8,$$
$$\zeta_{41} = H_2S_2(\zeta_4 + k\zeta_3)\zeta_5\xi_2\Upsilon_2\Upsilon_8,$$
$$\zeta_{42} = H_1S_1(\zeta_4 + k\zeta_3)\zeta_5\xi_1\Upsilon_2\Upsilon_8,$$
$$\zeta_{43} = H_2S_1(\zeta_4 + k\zeta_3)\zeta_5\xi_1\Upsilon_6,$$
$$\zeta_{44} = \zeta_5((k\zeta_1 + 1)\Upsilon_{10} + H_2S_2\xi_2(\zeta_4 + k\zeta_3))\Upsilon_3,$$
$$\zeta_{45} = (k\zeta_1 + 1)(S_1\zeta_6\Upsilon_1 + S_3\zeta_5\lambda_1)\Upsilon_{10},$$
$$\zeta_{46} = (k\zeta_1 + 1)(\zeta_6 + 2\zeta_5)\Upsilon_{10},$$
$$\zeta_{47} = (\zeta_4 + k\zeta_3)(\zeta_6\xi_2 - \zeta_7\xi_1)\Upsilon_1,$$
$$\zeta_{48} = (\zeta_4 + k\zeta_3)(S_3\zeta_5\lambda_1 + S_1\zeta_6)\xi_2,$$
$$\zeta_{49} = (\zeta_4 + k\zeta_3)\zeta_5(2S_2\xi_2 - S_4\lambda_2\xi_1),$$
$$\zeta_{50} = (\zeta_4 + k\zeta_3)(\zeta_7 + 2\zeta_5)\xi_1,$$
$$\zeta_{51} = (C_s\Upsilon_7 + C_h\tilde{C}_m\Upsilon_5)\Upsilon_8\Upsilon_9,$$
$$\zeta_{52} = H_1S_2(\zeta_4 + k\zeta_3)\xi_2\Upsilon_8,$$
$$\zeta_{53} = 2\tilde{C}_m(k\zeta_1 + 1)\Upsilon_6\Upsilon_9 + \zeta_{52},$$
$$\zeta_{54} = (k\zeta_1 + 1)(S_2\Upsilon_1 - S_4\lambda_2)\Upsilon_9,$$
$$\zeta_{55} = C_sH_2S_1(\zeta_4 + k\zeta_3)\xi_1\Upsilon_7\Upsilon_8,$$
$$\zeta_{56} = S_2(k\zeta_1 + 1)\Upsilon_9 - \zeta_{55},$$
$$\zeta_{57} = H_2S_1(\zeta_4 + k\zeta_3)\xi_1\Upsilon_5\Upsilon_8,$$
$$\zeta_{58} = (k\zeta_1 + 1)\Upsilon_{10}\Upsilon_4\Upsilon_8,$$
$$\zeta_{59} = H_2S_2(\zeta_4 + k\zeta_3)\xi_2\Upsilon_4\Upsilon_8,$$
$$\zeta_{60} = (k\zeta_1 + 1)\Upsilon_{10}\Upsilon_2\Upsilon_8,$$
$$\zeta_{61} = H_2S_2(\zeta_4 + k\zeta_3)\xi_2\Upsilon_2\Upsilon_8,$$
$$\zeta_{62} = (\zeta_4 + k\zeta_3)\xi_1\Upsilon_{10}\Upsilon_8,$$
$$\zeta_{63} = H_2S_1(\zeta_4 + k\zeta_3)\xi_1\Upsilon_6 - (k\zeta_1 + 1)\Upsilon_{10}\Upsilon_3,$$
$$\zeta_{64} = \tilde{C}_mH_2S_2(\zeta_4 + k\zeta_3)\xi_2\Upsilon_3 - S_1(k\zeta_1 + 1)\Upsilon_1\Upsilon_{10},$$
$$\zeta_{65} = (k\zeta_1 + 1)(S_3\lambda_1 + S_1)\Upsilon_{10},$$

$$\zeta_{66} = H_2 S_1 S_2 (\zeta_4 + k\zeta_3)(\xi_2 - \xi_1)\Upsilon_1,$$
$$\zeta_{67} = (\zeta_4 + k\zeta_3)(S_3\lambda_1 + S_1)\xi_2,$$
$$\zeta_{68} = (\zeta_4 + k\zeta_3)(S_4\lambda_2 + S_2)\xi_1,$$
$$\zeta_{69} = S_2\zeta_8 - 2C_s(\zeta_9 + \zeta_{10} + \zeta_{11}),$$
$$\zeta_{70} = -2\tilde{C}_m C_h(\zeta_{12} + \zeta_{13} + \zeta_{14}),$$
$$\zeta_{71} = 2H_2 S_2(C_s\zeta_{15} + \zeta_{17}) + \tilde{C}_m C_h k\zeta_{18},$$
$$\zeta_{72} = 2\tilde{C}_m C_h\zeta_{19} - S_1\zeta_{20} + \zeta_{21}\zeta_{22},$$
$$\zeta_{73} = 2\tilde{C}_m H_2(S_1\zeta_{22} + \zeta_{23} - S_2\zeta_{24}),$$
$$\zeta_{74} = 2H_2(S_1 S_2\zeta_{25} - S_1\zeta_6\zeta_{26} + S_4\zeta_{27}),$$
$$\zeta_{75} = -2H_2 S_2(S_3\zeta_{28} + \zeta_{29} + S_1\zeta_{30}),$$
$$\zeta_{76} = 2(\zeta_{34} - \zeta_{31} + \tilde{C}_m\zeta_{33}) + H_1 S_2\zeta_{32},$$
$$\zeta_{77} = 2(S_2\zeta_{35} + C_s\zeta_{38} - H_2 S_1\zeta_{36}\zeta_{37}),$$
$$\zeta_{78} = 2(C_s\zeta_{39} + \tilde{C}_m C_h\zeta_{40} + \tilde{C}_m C_h\zeta_{41}),$$
$$\zeta_{79} = 2\tilde{C}_m\zeta_{43} - H_1 S_1\zeta_{42} - 2\tilde{C}_m\zeta_{44},$$
$$\zeta_{80} = -2(\zeta_{45} + S_1\zeta_{46} + H_2 S_1 S_2\zeta_{47}),$$
$$\zeta_{81} = 2H_2(S_1 S_2\zeta_{50} - S_2\zeta_{48} - S_1\zeta_{49}),$$
$$\zeta_{82} = \zeta_{53} - 2(k\zeta_1 + 1)\zeta_{51},$$
$$\zeta_{83} = 2(\zeta_{56} - \zeta_{54}),$$
$$\zeta_{84} = 2(C_s\zeta_{59} + C_s\zeta_{58} - \tilde{C}_m C_h\zeta_{57}),$$
$$\zeta_{85} = 2\tilde{C}_m C_h(\zeta_{60} + \zeta_{61}) - H_1 S_1\zeta_{62},$$
$$\zeta_{86} = 2(\tilde{C}_m\zeta_{63} - \zeta_{64} - \zeta_{65}),$$
$$\zeta_{87} = 2(\zeta_{66} - H_2 S_2\zeta_{67} + H_2 S_1\zeta_{68}).$$

## References


1. S.P. Bakanov, *Thermophoresis in gases at small Knudsen numbers*, Aerosol Science and Technology, **15**, 77–92, 1991, https://doi.org/10.1080/02786829108959515.

2. F. Zheng, *Thermophoresis of spherical and non-spherical particles: A review of theories and experiments*, Advances in Colloid and Interface Science, **97**, 255–278, 2002, https://doi.org/10.1016/S0001-8686(01)00067-7.

3. E.H. Kennard, *Kinetic Theory of Gases*, McGraw-Hill, New York and London, 1938.

4. J. Brock, *On the theory of thermal forces acting on aerosol particles*, Journal of Colloid Science, **17**, 768–780, 1962, https://doi.org/10.1016/0095-8522(62)90051-X.

5. Y.C. CHANG, H.J. KEH, *Effects of thermal stress slip on thermophoresis and photophoresis*, Journal of Aerosol Science, **50**, 1–10, 2012, https://doi.org/10.1016/j.jaerosci.2012.03.006.

6. Y.C. CHANG, H.J. KEH, *Thermophoresis at small but finite Péclet numbers*, Aerosol Science and Technology, **52**, 1028–1036, 2018, https://doi.org/10.1080/02786826.2018.1498588.

7. Y.M. TSENG, H.J. KEH, *Thermophoresis of a cylindrical particle at small finite Péclet numbers*, Aerosol Science and Technology, **55**, 54–62, 2021, https://doi.org/10.1080/02786826.2020.1812504.

8. H.J. KEH, Y.C. CHANG, *Thermophoresis of an aerosol spheroid along its axis of revolution*, Physics of Fluids, **21**, 062001, 2009, https://doi.org/10.1063/1.3156002.

9. H.J. KEH, H.J. TU, *Thermophoresis and photophoresis of cylindrical particles*, Colloids and Surfaces A: Physicochemical and Engineering Aspects, **176**, 2-3, 213–223, 2001, https://doi.org/10.1016/S0927-7757(00)00567-7.

10. Y.C. CHANG, H.J. KEH, *Thermophoresis and photophoresis of an aerosol cylinder with thermal stress slip*, American Journal of Heat and Mass Transfer, **4**, 85–103, 2017, https://doi.org/10.7726/ajhmt.2017.1006.

11. L.J. WANG, H.J. KEH, *Boundary effects on thermophoresis of aerosol cylinders*, Journal of Aerosol Science, **41**, 771–789, 2010, https://doi.org/10.1016/j.jaerosci.2010.05.002.

12. S.Y. LU, C.T. LEE, *Thermophoretic motion of an aerosol particle in a non-concentric pore*, Journal of Aerosol Science, **32**, 1341–1358, 2001, https://doi.org/10.1016/S0021-8502(01)00054-4.

13. H.J. KEH, P.Y. CHEN, *Thermophoresis of an aerosol sphere parallel to one or two plane walls*, AIChE Journal, **49**, 2283–2299, 2003, https://doi.org/10.1002/aic.690490906.

14. H.J. KEH, Y.C. CHANG, *Thermophoresis of an aerosol sphere perpendicular to two plane walls*, AIChE Journal, **52**, 1690–1704, 2006, https://doi.org/10.1002/aic.10788.

15. D.A. NIELD, A. BEJAN, *Convection in Porous Media*, Springer, New York, 2006.

16. P.K. YADAV, A. TIWARI, S. DEO, A. FILIPPOV, S. VASIN, *Hydrodynamic permeability of membranes built up by spherical particles covered by porous shells: effect of stress jump condition*, Acta Mechanica, **215**, 193–209, 2010, https://doi.org/10.1007/s00707-010-0331-8.

17. P.K. YADAV, S. DEO, M.K. YADAV, A. FILIPPOV, *On hydrodynamic permeability of a membrane built up by porous deformed spheroidal particles*, Colloid Journal, **75**, 611–622, 2013, https://doi.org/10.1134/S1061933X13050165.

18. P.K. YADAV, S. DEO, *Stokes flow past a porous spheroid embedded in another porous medium*, Meccanica, **47**, 1499–1516, 2012, https://doi.org/10.1007/s11012-011-9533-y.

19. K.E. RAGAB, M.S. FALTAS, M.A. SAAD, *Modeling thermophoretic transport of a colloidal particle in porous media with planar wall constraints*, Physics of Fluids, **37**, 082026, 2025, https://doi.org/10.1063/5.0280178.

20. M.S. FALTAS, K.E. RAGAB, *Thermophoretic and photophoretic velocities and forces of a spherical particle embedded in Brinkman medium*, European Physical Journal Plus, **134**, 475, 2019, https://doi.org/10.1140/epjp/i2019-12855-y.

21. M.S. Faltas, K.E. Ragab, *Thermophoresis of cylindrical particle immersed in Brinkman fluid*, Colloid Journal, **83**, 676–687, 2021, https://doi.org/10.1134/S1061933X2106003X.

22. M.S. Faltas, H.H. Sherief, A.A. Allam, M.G. Nashwan, M. El-Sayed, *Thermophoresis of a spherical particle in a permeable microchannel with thermal stress slip*, Physical Review Fluids, **8**, 054102, 2023, https://doi.org/10.1103/PhysRevFluids.8.054102.

23. B.C. Prasannakumara, J.K. Madhukesh, G.K. Ramesh, *Bioconvective nanofluid flow over an exponential stretched sheet with thermophoretic particle deposition*, Propulsion and Power Research, **12**, 284–296, 2023, https://doi.org/10.1016/j.jppr.2023.05.004.

24. M.S. Faltas, H.H. Sherief, M.M. Ismail, *Thermophoresis migration of an aerosol spherical particle embedded in a Brinkman medium at small non-zero Péclet numbers*, Physics of Fluids, **35**, 2023, https://doi.org/10.1063/5.0160402.

25. J.S. Huang, H.H. Hsu, *Effect of thermophoresis on particle deposition on an inclined plate in variable viscosity fluid flow with in a porous medium*, Case Studies in Thermal Engineering, **67**, 105813, 2025, https://doi.org/10.1016/j.csite.2025.105813.

26. S. Nishad, K.P. Madasu, *Thermophoresis of an aerosol cylinder in Brinkman medium within a cylindrical cavity*, Archive of Mechanical Engineering, **72**, 177–198, 2025, https://doi.org/10.24425/ame.2025.153735.

27. A.C. Eringen, *Microcontinuum Field Theories II: Fluent Media*, Springer Science and Business Media, New York, 2001.

28. S. El-Sapa, M.S. Faltas, K.E. Ragab, *Oscillatory Brinkman-micropolar electroosmosis in cylindrical microannuli*, Chinese Journal of Physics, **97**, 1464–1491, 2025, https://doi.org/10.1016/j.cjph.2025.08.015.

29. E.I. Saad, M.S. Faltas, *Theory of thermophoresis of a spherical particle embedded in a micropolar fluid*, Journal of Molecular Liquids, **282**, 527–544, 2019, https://doi.org/10.1016/j.molliq.2019.02.118.

30. E.I. Saad, M.S. Faltas, *Thermophoresis of a spherical particle straddling the interface of a semi-infinite micropolar fluid*, Journal of Molecular Liquids, **312**, 113289, 2020, https://doi.org/10.1016/j.molliq.2020.113289.

31. P. Roja, T. Reddy, S.M. Ibrahim, G. Lorenzini, N.A.C. Sidik, *The effect of thermophoresis on MHD stream of a micropolar liquid through a porous medium with variable heat and mass flux and thermal radiation*, CFD Letters, **14**, 118–136, 2022, https://doi.org/10.37934/cfdl.14.4.118136.

32. W. Liu, J. Wang, G. Xia, Z. Li, *Thermophoresis of nanoparticles in the transition regime*, Physics of Fluids, **35**, 083316, 2023, https://doi.org/10.1063/5.0161744.

33. S. Nishad, K.P. Madasu, *Axisymmetric migration of an aerosol sphere in bounded micropolar fluid: thermophoresis effect*, Journal of the Brazilian Society of Mechanical Sciences and Engineering, **47**, 144, 2025, https://doi.org/10.1007/s40430-025-05416-0.

34. N. Sarma, A. Paul, B. Patgiri, *Numerical analysis of maxwell hybrid nanofluid flow implementing modified Fourier–Fick's model through an unsteady vertical cylinder with brownian motion and thermophoresis*, Journal of the Brazilian Society of Mechanical Sciences and Engineering, **47**, 1–17, 2025, https://doi.org/10.1007/s40430-025-05722-7.

35. A. SINGH, P.K. YADAV, *Analysis of bio-convective ternary hybrid nanofluid flow in atherosclerotic bifurcated artery: A numerical approach*, Computer Methods and Programs in Biomedicine, **273**, 109129, 2026, https://doi.org/10.1016/j.cmpb.2025.109129.

36. P. SRIVASTAVA, P.K. YADAV, *Brinkman–Forchheimer model for unsteady mixed convective magnetohydrodynamics flow of couple stress fluid through swarm of particles at high magnetic Reynold number: Cell model technique*, Chemical Engineering Science, **321**, 122758, 2026, https://doi.org/10.1016/j.ces.2025.122758.

37. A.M. ABD-ALLA, I.A. ABBAS, S.M. ABO-DHAB, Y. ELMHEDY, H. SAPOOR, M.A. ABDELHAFEZ, *Effect of magnetic field and heat transfer on peristaltic flow of a micropolar fluid through a porous medium*, Waves in Random and Complex Media, **35**, 2, 4070–4081, 2025, https://doi.org/10.1080/17455030.2022.2058111.

38. N.A. KHAN, M. SULAIMAN, *Heat transfer and thermal conductivity of magneto micropolar fluid with thermal non-equilibrium condition passing through the vertical porous medium*, Waves in Random and Complex Media, **35**, 5, 9735–9759, 2025, https://doi.org/10.1080/17455030.2022.2108161.

39. M.S. KAUSAR, A.B.M. ALI, T. ANWAR, A. SOTTAROV, T. WALELIGN, M. WAQAS, *A computational framework for micropolar fluid considering chemical reaction in porous media with stagnation point flow over a stretchable sheet in the presence of viscous dissipation*, International Journal of Thermofluids, **30**, 101453, 2025, https://doi.org/10.1016/j.ijft.2025.101453.

40. S. AHAMEDSHERIFF, V. RAJARAM, G. MANI, S.T.M. THABET, I. KEDIM, *Impacts of soret and dufour possessions on micropolar fluid past a stretching sheet in a porous medium*, Scientific Reports, **15**, 33059, 2025, https://doi.org/10.1038/s41598-025-18302-5.

41. A. KUMAR, P.K. YADAV, *Heat and mass transfer analysis of non-miscible couple stress and micropolar fluids flow through a porous saturated channel*, Journal of Applied Mathematics and Mechanics, **104**, e202300635, 2024, https://doi.org/10.1002/zamm.202300635.

42. L. KUMAR, A. SINGH, V.K. JOSHI, K. SHARMA, *MHD micropolar fluid flow with hall current over a permeable stretching sheet under the impact of Dufour–Soret and chemical reaction*, International Journal of Thermofluids, **26**, 101042, 2025, https://doi.org/10.1016/j.ijft.2024.101042.

43. S. NISHAD, K.P. MADASU, *Motion of an aerosol sphere in hydrogel medium under thermal gradient*, Archives of Mechanics, **77**, 2, 177–212, 2025, https://doi.org/10.24423/aom.4587.

44. S. NISHAD, K.P. MADASU, *Boundary effects on thermophoretic migration of a spherical particle in Brinkman micropolar fluid within a cavity*, Physics of Fluids, **37**, 082067, 2025, https://doi.org/10.1063/5.0285728.

45. M.T. KAMEL, D. ROACH, M.H. HAMDAN, *On the micropolar fluid flow through porous media*, Proceedings of the 11$^{\text{th}}$ WSEAS International Conference on Mathematical Methods, Computational Techniques and Inteligent Systems, 190–197, 2009.

46. K.P. MADASU, D. SRINIVASACHARYA, *Micropolar fluid flow through a cylinder and a sphere embedded in a porous medium*, International Journal of Fluid Mechanics Research, **44**, 3, 229–240, 2017, https://doi.org/10.1615/InterJFluidMechRes.2017015283.

47. D.Y. Khanukaeva, A.N. Filippov, *Isothermal flows of micropolar liquids: Formulation of problems and analytical solutions*, Colloid Journal, **80**, 4–36, 2018, https://doi.org/10.1134/S1061933X18010040.

48. S. El-Sapa, *Effect of permeability of Brinkman flow on thermophoresis of a particle in a spherical cavity*, European Journal of Mechanics B/Fluids, **79**, 315–323, 2020, https://doi.org/10.1016/j.euromeChflu.2019.09.017.

49. L. Talbot, R.K. Cheng, R.W. Schefer, D.R. Willis, *Thermophoresis of particles in a heated boundary layer*, Journal of Fluid Mechanics **101**, 737–758, 1980, https://doi.org/10.1017/S0022112080001905.

*Received September 18, 2025; revised version December 26, 2025.*
*Published online January 28, 2026.*